Finite Elements in Analysis and Design 45 (2009) 852–860

Contents lists available at ScienceDirect

Finite Elements in Analysis and Design

journal homepage: www.elsevier.com/locate/finel

# Optimization of dynamic behaviors of an orthotropic composite shell subjected to hygrothermal environment

H.K. Cho*

*Satellite Technology Research Center, Korea Advanced Institute of Science and Technology, 373-1 Guseong-dong, Yuseong-gu, Daejeon 305-701, Republic of Korea*

ARTICLE INFO

*Article history:*
Received 23 June 2008
Received in revised form 18 June 2009
Accepted 22 June 2009
Available online 29 July 2009

*Keywords:*
Dynamics
Shell
Optimization
Composite materials
Hygrothermal analysis

ABSTRACT

Dynamic responses of an orthotropic plate subjected to hygrothermal environments have been optimized. Non-gradient evolutionary genetic algorithm (GA) is employed to optimize dynamic behaviors of orthotropic composite. Presented optimization scheme, whose approach is advantageously conducted in conjunction with FEA, involves controlling locally fiber directions from element to element. The geometry is discretized into specially developed 3D shell composite elements which are able to handle hygrothermal effects of our own design. Shell, rather than plate, elements enable one to reliable account for features such as membrane and bending stress variations through the plate. By using the specially developed shell element, dynamic deflection and natural frequency are minimized by optimizing design variables which are local fiber directions within discrete finite elements. Since fiber orientations are optimized locally within a plate, the technique provides more than just a favorable ply angle of fiber reinforced rectilinearly orthotropic plate. Results presented, not available so far, could be useful to ascertain the effects of locally varying fiber direction on dynamic analysis under temperature and humidity boundary conditions.



## 1. Introduction

Associated with their favorable response, fiber reinforced composites find widespread utilization. Their high strength- and stiffness-to-weight ratios, and design flexibility, foster engineering use of composites. In particular, composite plates are becoming increasingly prevalent in aerospace and transportation components which are dynamically loaded in diversified environments. Many recent studies [1–9] have focused on a dynamic analysis of composite, including their improvement and optimization. Practical composite structures are often subjected to environmental conditions during their life cycle. Moisture and temperature changes affect the stiffness and strength of composites, and their static and dynamic behaviors can depend significantly on such hygrothermal conditions. Experimental results show [10] that composite modulus and strength typically decrease with increased temperature and moisture. Hygrothermally induced dissimilar lamina expansions can also introduce residual stress. Sinha et al. [1,2,5] used nonlinear transient plate theory to study composites in hygrothermal environments, Lee and Yen [11] analyzed hygrothermal effects on the stability of a composite panel. The inevitable use of fiber reinforced orthotropic composites in hygrothermal environments renders it imperative to be able to analyze coupled problems of hygro-thermo-mechanically loaded composite structures. Optimization technologies are also effective for designing enhanced orthotropic composite members [7,12–16].

The first task is to extend nonlinear, dynamic FEA of orthotropic composites operating in a hygrothermal environment using a degenerated shell element. Conventional finite-element formulation is modified to include the energy resulting from all types of initial stresses, such as compression, bending, etc., induced by moisture or temperature changes. Using a genetic algorithm, the design is then optimized by minimizing either the largest displacements or the dynamic responses, i.e., minimize the fundamental natural frequency, by controlling the fiber direction independently in respective finite elements of a plane. Fiber direction can vary from element-to-element and the design variables are the fiber direction within individual elements. The number of design variables is therefore the same as the total number of the elements. Fiber reinforced composites have been optimized previously utilizing a GA. Holland [17] and Goldberg [18] formulated the engineering basis for implementing GA, while applications to composite design were conducted by Haftka, Gürdal, Hajela and Cho et al. [15,16,19,20]. GA is a probabilistic optimization method which uses biological concepts, including Darwin's principal of survival of the fittest. Unlike many conventional search algorithms which move from one point to another along the steepest gradient line in the design variable space, genetic algorithms employ a population. The ability of the GA's multi-point

* Tel.: +82 42 869 8617; fax: +82 42 861 0064.
*E-mail address:* marklee1@hanmail.net (H.K. Cho).

0168-874X/$ - see front matter © 2009 Elsevier B.V. All rights reserved.
doi:10.1016/j.finel.2009.06.029

discrete search technique to reach a global, rather than potentially just a *local*, design space, is highly effective and a major attribute of this method, over other optimization schemes.

Sinha and coworkers [2,5] presented dynamic analyses of delaminated composites with hygrothermal effects. However, previous analyses appear to be restricted to plate theory and relatively uncomplicated geometries such as squares or rectangles having simple boundary conditions. Using plate theory renders such analyses only effective for flat shapes, on the other hand, the present use of three-dimensional, arbitrary-surface, newly developed shell (rather than plate) elements, combined with GA optimization algorithm, greatly expands the scope of application. The importance of the special shell element formulated here, its synergism with the GA, and robustness and accuracy of the approach are emphasized by illustrative examples. This study involved developing and integrated optimization program, named COMDO8 (COMposite Dynamic Optimization code: 3-D 8-node degenerated shell element), which combines a FEA module, hygro-thermo-mechanical nonlinear dynamics and a GA module to compute simultaneously the object function.

## 2. Analytical background

### 2.1. Degenerated shell element for laminated composite [21–26]

Motivated by the current desire to synergize FEA and optimization abilities numerically, a general serendipity isoparametric degenerated 8-node shell element was specially developed for the present fiber reinforced (transversely isotropic) composite study. Based on general shell theory, the element is suitable for modeling curved shallow composite plates. The isoparametric shell element is very attractive as it is highly effective for analyzing a variety of plates and shell situations. Shell geometry is represented by the coordinates and normal vectors of its middle surface, Fig. 1. Each node of an element has five degrees of freedom: three translations ($u$, $v$, $w$) in the directions of the global $x$, $y$ and $z$ axes and two rotations ($\alpha$, $\beta$) with respect to the axes in the plane of the middle surface, Fig. 1. Our shell element employs total Lagrangian nonlinear incremental formulation of a continuous medium [21,23,25].

Unit vectors $e_r, e_s, e_t$ of Fig. 1 are typically not orthogonal, whereas $e_{\bar{r}}, e_{\bar{s}}, e_t$ are orthogonal. Using the natural coordinates $r$, $s$, and $t$, the global Cartesian coordinates $x$, $y$, $z$ and displacement at any location in the element having $q$ nodal points are

$$
\begin{aligned}
x(r,s,t) &= \sum_{k=1}^{q} N_k x_k + \frac{t}{2}\sum_{k=1}^{q} a_k N_k V_{nx}^k \\
u(r,s,t) &= \sum_{k=1}^{q} N_k u_k + \frac{t}{2}\sum_{k=1}^{q} a_k N_k (-{}^0V_{2x}^k \alpha_k + {}^0V_{1x}^k \beta_k) \\
y(r,s,t) &= \sum_{k=1}^{q} N_k y_k + \frac{t}{2}\sum_{k=1}^{q} a_k N_k V_{ny}^k \\
v(r,s,t) &= \sum_{k=1}^{q} N_k v_k + \frac{t}{2}\sum_{k=1}^{q} a_k N_k (-{}^0V_{2y}^k \alpha_k + {}^0V_{1y}^k \beta_k) \\
z(r,s,t) &= \sum_{k=1}^{q} N_k z_k + \frac{t}{2}\sum_{k=1}^{q} a_k N_k V_{nz}^k \\
w(r,s,t) &= \sum_{k=1}^{q} N_k w_k + \frac{t}{2}\sum_{k=1}^{q} a_k N_k (-{}^0V_{2z}^k \alpha_k + {}^0V_{1z}^k \beta_k)
\end{aligned} \tag{1}
$$

where $N_k(r,s)$ is the interpolation (shape) function associated with node $k$, $a_k$ is shell thickness in $t$ direction at nodal point $k$, and $V_{ni}^k$ represents the $i$th component of unit vector $V_n^k$ "normal" to the shell's mid-surface in the direction $t$ at nodal point $k$. $\alpha_k$ and $\beta_k$ are rotations of the normal vector.

The virtual work principle is applied to the deformable shell under arbitrary dynamic equilibrium condition at time $t$. The external virtual work (energy) at time $t$, ${}^tR$, can be expressed as [21]

$$
{}^tR = \int_{{}^0V} {}^t_0\ddot{u}_i\, {}^0\rho\, \delta^t_0 u_i\, {}^0dV + \int_{{}^0V} {}^t_0S_{ij}\, \delta^t_0\varepsilon_{ij}\, {}^0dV \tag{2}
$$

where ${}^t_0S_{ij}$ is the 2nd Piola–Kirchhoff stress tensor or nominal (engineering) stress, and ${}^t_0\varepsilon_{ij}$ and ${}^0\rho$ are strain tensor and mass density, respectively. The relationship between the 2nd Piola–Kirchhoff stress tensor and Green–Lagrange strain tensor, ${}^t_0\varepsilon_{ij}$ , is ${}^t_0S_{ij} = {}^t_0C_{ijrs}\,{}^t_0\varepsilon_{rs}$ such that ${}^t_0C_{ijrs}$ represents material properties tensor. The stress–strain relationship based on the shell local coordinate system is $\{\sigma\} = [C'_{sh}]\{\varepsilon\}$. For orthotropic materials [22–24],

$$
[C'_{sh}] = \begin{bmatrix}
\bar{C}_{11} & \bar{C}_{12} & 0 & \bar{C}_{14} & 0 & 0 \\
\bar{C}_{21} & \bar{C}_{22} & 0 & \bar{C}_{24} & 0 & 0 \\
0 & 0 & 0 & 0 & 0 & 0 \\
\bar{C}_{41} & \bar{C}_{42} & 0 & \bar{C}_{44} & 0 & 0 \\
0 & 0 & 0 & 0 & \bar{C}_{55} & \bar{C}_{56} \\
0 & 0 & 0 & 0 & \bar{C}_{65} & \bar{C}_{66}
\end{bmatrix} \tag{3}
$$

where material stiffness matrix $[C'_{sh}]$ is referred to the local coordinates axis $(\bar{r}, \bar{s}, t)$ of an individual element. For evaluating the element stiffness, the material matrix in terms of local coordinates $(\bar{r}, \bar{s}, t)$ must be transformed to that, $[C_{sh}]$, in the global system $(x, y, z)$ using $[C_{sh}] = [T_{sh}]^T[C'_{sh}][T_{sh}]$ [26]. The elements of the transformation matrix $[T_{sh}]$, are obtained from the direction cosines of the $\bar{r}, \bar{s}, t$ coordinate axes measured in the $x, y, z$ coordinate directions. The Green–Lagrange strain tensor at time $t$, ${}^t_0\varepsilon_{ij}$, can be divided into the linear, $e_{ij}$, and the nonlinear, $\eta_{ij}$, terms [21].

$$
\begin{aligned}
&{}^t_0\varepsilon_{ij} = {}^t_0e_{ij} + {}^t_0\eta_{ij} \\
&{}^t_0e_{ij} = \tfrac{1}{2}({}^t_0u_{i,j} + {}^t_0u_{j,i}) = [{}^t_0B_{L0}]\{{}^t_0u\} \\
&{}^t_0\eta_{ij} = \tfrac{1}{2}({}^t_0u_{k,i} \cdot {}^t_0u_{k,j}) = [{}^t_0B_{L2}]\{{}^t_0u\}
\end{aligned} \tag{4}
$$

where $[B_{L0}]$ and $[B_{L2}]$ are linear and nonlinear component of strain–displacement transformation matrix, respectively (see details in Ref. [21]).

### 2.2. Hygrothermal constitutive relationships [1,2,5,11,21]

The temperature and/or moisture are assumed to be uniform (spatially and temporally) once they have reached equilibrium. The general form of stress–strain relationship for an orthotropic media in which temperature and moisture effects are considered is

$$
\begin{Bmatrix} \sigma_{xx} \\ \sigma_{yy} \\ \sigma_{zz} \\ \tau_{xy} \\ \tau_{yz} \\ \tau_{xz} \end{Bmatrix} = [C_{sh}] \begin{Bmatrix} \varepsilon_{xx} - \alpha^T_{xx}\Delta T - \beta^H_{xx}\Delta M \\ \varepsilon_{yy} - \alpha^T_{yy}\Delta T - \beta^H_{yy}\Delta M \\ \varepsilon_{zz} - \alpha^T_{zz}\Delta T - \beta^H_{zz}\Delta M \\ \gamma_{xy} - \alpha^T_{xy}\Delta T - \beta^H_{xy}\Delta M \\ \gamma_{yz} \\ \gamma_{xz} \end{Bmatrix} \tag{5}
$$

where $\Delta T$ is the temperature rise, $\Delta M$ is the increase in moisture content (moisture concentration weight/specific weight). The hygro coefficients, $\beta^H$, (swelling or concentration) are directly dependent in the same manner as are the thermal coefficients, $\alpha^T$.

If the temperature and moisture corresponding to the stress-free state is $T_0$ and $M_0$, respectively, one can evaluate the nodal point

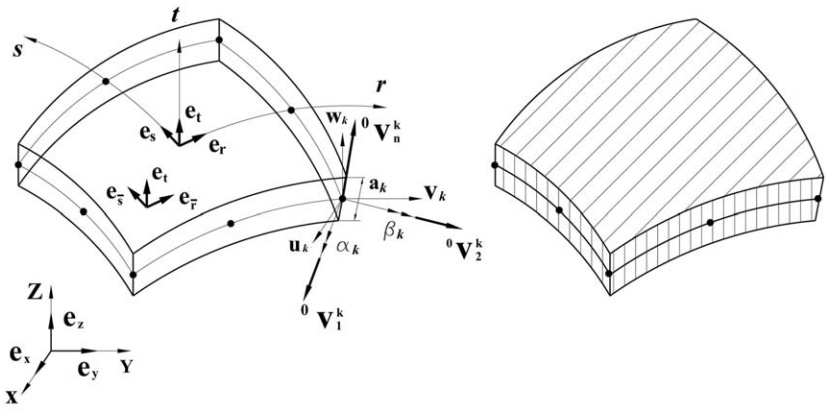


**Fig. 1.** Eight-node degenerated shell element.

forces to which the element must be subjected under $\Delta T$ and $\Delta M$ in order that there are no nodal point displacements. The stresses due to the hygrothermal strains can be thought of as initial/residual stresses (i.e., hygrothermally induced stresses equivalent to those one would have to apply mechanically to produce these same hygrothermal strains). The nodal point forces are thus $R_I = \int_V [B_{L0} + B_{L1}]^T \sigma^I \, dV$ and the initial stresses are

$$\sigma^I = -[C_{sh}] \left\{ \{\alpha_{xx}^T \ \alpha_{yy}^T \ \alpha_{zz}^T \ \alpha_{xy}^T \ 0 \ 0\}^T \left\{ \left( \sum_{k=1}^{q} N_k T_k \right) - T_0 \right\} + \{\beta_{xx}^T \ \beta_{yy}^T \ \beta_{zz}^T \ \beta_{xy}^T \ 0 \ 0\}^T \left\{ \left( \sum_{k=1}^{q} N_k M_k \right) - M_0 \right\} \right\} \tag{6}$$

Analytical handling of stresses resulting from moisture changes is analogous to that due to thermal effects except one replaces thermal coefficients with moisture coefficients. Values of the elastic properties and thermal and moisture coefficients are assumed to be independent of the present temperature or moisture changes.

### 2.3. Finite element formulation for nonlinear dynamic analysis

This study uses Newmark's implicit time integration method for the nonlinear dynamic analysis. Newmark originally proposed, as an unconditionally stable scheme, the constant-average-acceleration method (trapezoidal rule) in which case $\gamma = 0.25$, $\delta = 0.5$ in Eq. (7). Quantities $\gamma$ and $\delta$ are parameters that can be determined to obtain integration accuracy and stability. The Newmark integration scheme can be viewed as an extension of the linear acceleration method. Using the trapezoidal rule of time integration and $\gamma$=0.25 and $\delta$=0.5, the general displacements, $U$, employ the following assumptions:

$$^{t+\Delta t}U = {}^tU + {}^t\dot{U}\Delta t + [(\tfrac{1}{2} - \gamma)^t\ddot{U} + \gamma^{t+\Delta t}\ddot{U}]\Delta t^2$$

$$^{t+\Delta t}\dot{U} = {}^t\dot{U} + [(1-\delta)^t\ddot{U} + \delta^{t+\Delta t}\ddot{U}]\Delta t$$

$$^{t+\Delta t}\ddot{U}^{(i)} = \frac{4}{\Delta t^2}({}^{t+\Delta t}\ddot{U}^{(i-1)} - {}^tU - \Delta U^{(i)}) - \frac{4}{\Delta t}{}^tU - {}^t\ddot{U} \tag{7}$$

Combining Eqs. (2) and (4), and linearizing the resulting equation, gives

$$\int_{0V} {}^t_0\ddot{u}_i \, {}^0\rho \delta {}^t_0u_i \, {}^0dV + \int_{0V} {}_0C_{ijrs} \, {}^0e_{rs} \delta {}_0e_{ij} \, {}^0dV + \int_{0V} {}^t_0S_{ij} \delta {}_0\eta_{ij} \, {}^0dV = {}^{t+\Delta t}R - \int_{0V} {}^t_0S_{ij} \delta {}_0e_{ij} \, {}^0dV \tag{8}$$

Substituting Eq. (7) into Eq. (8), and discretizing the structure into finite elements so as to rewrite the resulting equation in terms of the shape function, enables one to express the linearized equilibrium equation of dynamics, Eq. (8), in Newton–Raphson nonlinear incremental matrix form. Moreover, the hygrothermal effects can now be included by adding equivalent initial stiffness terms to the global stiffness. The structure's deformation, stress, and strain tensors at time $t + \Delta t$ can be obtained by matrix calculations. The following Eq. (9) is the FEA equilibrium equation for the nonlinear dynamic analysis which includes hygrothermal effects.

$$\left( [{}^t_0K_L + {}^t_0K_{NL} + {}^t_0K_{th} + {}^t_0K_{hy}] + \frac{4}{\Delta t^2}[M] + \frac{2}{\Delta t^2}[C_{damp}] \right) \Delta U^{(i)} = {}^{t+\Delta t}R - {}^{t+\Delta t}_0F^{(i-1)} - [M]\left\{ \frac{4}{\Delta t^2}({}^{t+\Delta t}U^{(i-1)} - {}^tU) - \frac{4}{\Delta t}{}^t\dot{U} - {}^t\ddot{U} \right\} - [C_{damp}]\left\{ \frac{2}{\Delta t}({}^{t+\Delta t}U^{(i-1)} - {}^tU) - {}^t\dot{U} \right\} \tag{9}$$

with

$$[{}^t_0K_L] = \int_{0V} \begin{bmatrix} ([{}^t_0B_{L0}] + [{}^t_0B_{L1}])^T [C_{sh}] \\ ([{}^t_0B_{L0}] + [{}^t_0B_{L1}]) \end{bmatrix} {}^0dV$$

$$[{}^t_0K_{NL}] = \int_{0V} [[{}^t_0B_{NL}]^T [{}^t_0S][{}^t_0B_{NL}]] \, {}^0dV$$

$$\{{}^{t+\Delta t}_0F\} = \int_{0V} [([{}^{t+\Delta t}_0B_{L0}] + [{}^{t+\Delta t}_0B_{L1}])^T]_{(j)} \{{}^{t+\Delta t}_0\hat{S}\} \, {}^0dV$$

$$[M] = \int_{0V} [N]^T {}^0\rho [N] \, {}^0dV \tag{10}$$

Quantities $[K_L]$, $[K_{NL}]$, $[C_{damp}]$ and $\{F\}$ denote the linear and nonlinear terms of the stiffness matrix, damping coefficient matrix and internal nodal force vector, respectively. The right-hand term of Eq. (9) represents the residual force based on the virtual work theory, $[B_{L1}]$ is two times $[B_{L2}]$, $[B_{NL}]$ is nonlinear strain–displacement transformation matrix [21]. Rayleigh damping, $[C_{damp}] = a[M] + b[K]$, is employed. Relevant matrix details are presented in Ref. [21]. The initial stress stiffness matrices caused by the temperature and moisture can be expressed as

$$[{}^t_0K_{th}] = \int_{0V} \{[{}^t_0B_{NL}]^T [{}^t_0S_{th}][{}^t_0B_{NL}]\} \, {}^0dV$$

$$[{}^t_0K_{hy}] = \int_{0V} \{[{}^t_0B_{NL}]^T [{}^t_0S_{hy}][{}^t_0B_{NL}]\} \, {}^0dV \tag{11}$$

where $[S_{th}]$ and $[S_{hy}]$ are initial stress matrices due to the thermal and hygro effects, respectively.

## 3. Application

A number of literatures analyses the dynamic performance and optimization of mechanically loaded laminates. All plies of those laminate were rectilinear throughout the plate. This study extends such optimization concepts by allowing the fiber orientation to vary locally. The nonlinear dynamic analysis of a square orthotropic panel subjected to moisture and temperature effects is conducted and its mechanical behaviors (dynamic deflection and fundamental natural frequencies) are optimized. The objective functions are the maximum displacement at loading point 'A' and the fundamental natural frequency. The orthotropic composite is a typical fiber reinforced carbon epoxy material. A 50 mm×50 mm square panel with 3 mm thickness is discretized into 16 shell elements, Fig. 2. One edge is fixed and a point load of 100 N is applied suddenly (and remains constant thereafter with time) to a corner of the opposite edge. Moisture ($\Delta M = 0.25\%$) and temperature ($\Delta T = 125$ K) changes are included. Material properties are again considered to be independent of the moisture and temperature, Table 1. Fiber orientation ($\theta$) is measured from local element $x$-axis, which coincides with that of global $x$-axis at initial state, to principal material axis and is constant within an element. The fiber angle is initially set to zero through the plate. The aim of this study is to optimize the fiber directions within the single-ply, vertical point-loaded square orthotropic composite so as to minimize either the deflection at loading point 'A' (Case I) or the fundamental natural frequency ($f_1$), independently (Case II).

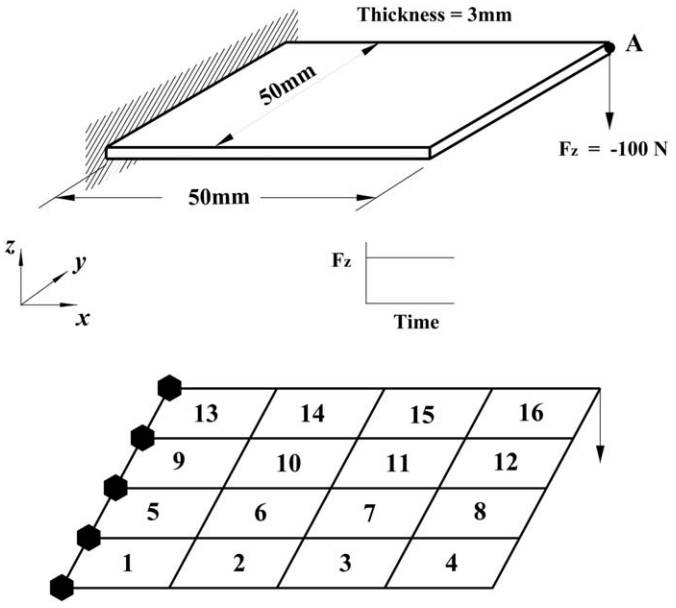


**Fig. 2.** Model geometry and boundary conditions for FEA orthotropic plate.

**Table 1**
Material properties of orthotropic carbon/epoxy composite [22].

| Properties | Carbon epoxy (C/E) |
|---|---|
| $E_{11}$ | 172.5 GPa |
| $E_{22} = E_{33}$ | 6.9 GPa |
| $\upsilon_{12} = \upsilon_{13}$ | 0.25 |
| $\upsilon_{23}$ | 0.22 |
| $G_{12} = G_{13}$ | 3.45 GPa |
| $G_{23}$ | 1.38 GPa |
| $\rho$ | 1600 kg m$^{-3}$ |
| $\alpha_1^T$, $\alpha_2^T$ | −0.3e−6 m/m K, 28.1e−6 m/m K |
| $\beta_1^H$, $\beta_2^H$ | 0.0, 0.44 |
| [C] (Damping matrix) | 1.e−2[$M$]+1.e−5[$K$] |

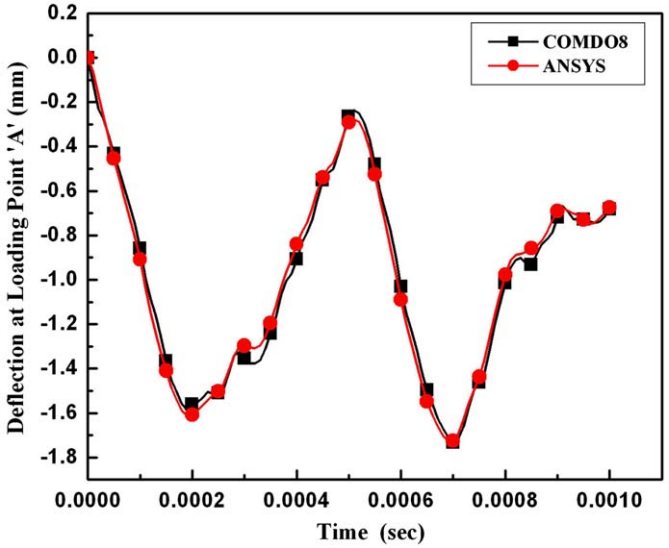


**Fig. 3.** Deflection at loading point 'A' of square panel of Fig. 2 without damping (fiber angle is zero).

Four situations are analyzed for each of these two optimization, cases : (i) point load ($F_Z = -100$ N at point 'A') only, (ii) point load ($F_Z = -100$ N at point 'A')+moisture ($\Delta M = 0.25\%$), (iii) point load ($F_Z = -100$ N at point 'A')+temperature ($\Delta T = 125$ K) and (iv) point load ($F_Z = -100$ N at point 'A')+moisture($\Delta M = 0.25\%$)+temperature ($\Delta T = 125$ K). Somewhat as in author's reference Cho and Rowlands [20], attention is focused here primarily on applying GA to control each element's fiber angle in nonlinear dynamic problems of orthotropic composites subjected to hygrothermal environments.

Minimizing the deflection at point 'A' (Case I) or fundamental natural frequency ($f_1$) (Case II) of the orthotropic panel of Fig. 2 and Table 1 for the given material, dimensions and boundary conditions was achieved by independently changing the fiber orientations within each element. These fiber directions, $\theta_i$, are the only design variables. Since the square panel of Fig. 2 is modeled by 16 elements, there are 16 design variables. Fiber direction within the element influences the stiffness and thereby changes the mechanical characteristics. The ultimate aim is to minimize dynamic deflection (Case I) or the first natural frequency (Case II) to satisfy design requirements of the given geometry, boundary conditions and hygrothermal operating environments by adjusting the local stiffness through locally varying fiber orientation. GA optimization is again utilized.

Many numerical optimization algorithms have been developed for engineering purpose. Each of them has it own peculiar capability. However, one has no optimization choice but to select non-gradient GA or something like that for this problem. Design solution fields of complicated coupled problems such as this one involving extensive nonlinearity, mechanical orthotropy, hygro-thermo-mechanical loading, many design variables, and dynamics is extremely challenging. Conventional optimization algorithms based on gradient searching method are inadequate for such a problem. Gradient searching methods are more likely to be entrapped into local convex or concave design space and are incapable of handling deep or stiff gradient hills of a (such as occur here) solution field. On the other hand GA searches the global optimum probabilistically with many searching points. GA capability is consequently not affected and/or diminished by the state of the design field.

The time increment $\Delta t$ used here is 1.0E−5 s and Rayleigh damping is employed. In order to substantiate the accuracy of the developed FEA code COMDO8 used, the nonlinear dynamic responses of the square panel excited by 100 N step load is first compared with

ANSYS results for both damped and undamped cases in Figs. 3 and 4, respectively. Results of Figs. 3 and 4 illustrate COMDO8's reliability. Fig. 5 shows the dynamic history of the deflection at point 'A' of the plate of Fig. 2 for mechanical loading with, and without, the hygrothermal environment. ANSYS is unable to handle the transient mechanical loading in the hygrothermal environments of Fig. 5.

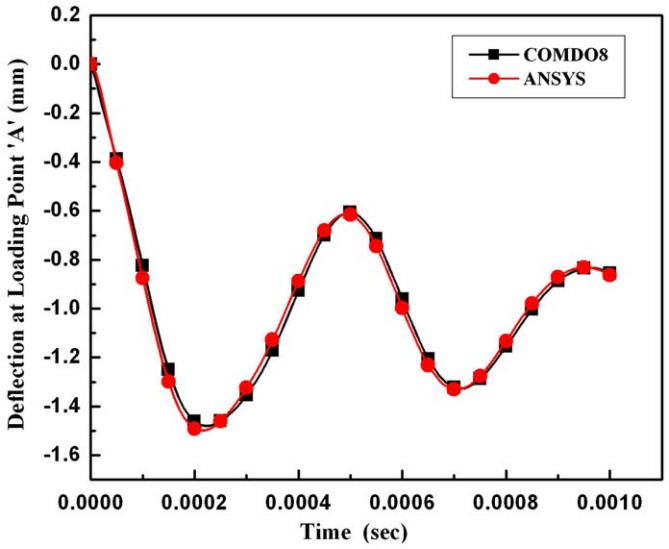


**Fig. 4.** Deflection at loading point 'A' of square panel of Fig. 2 with damping (fiber angle is zero).

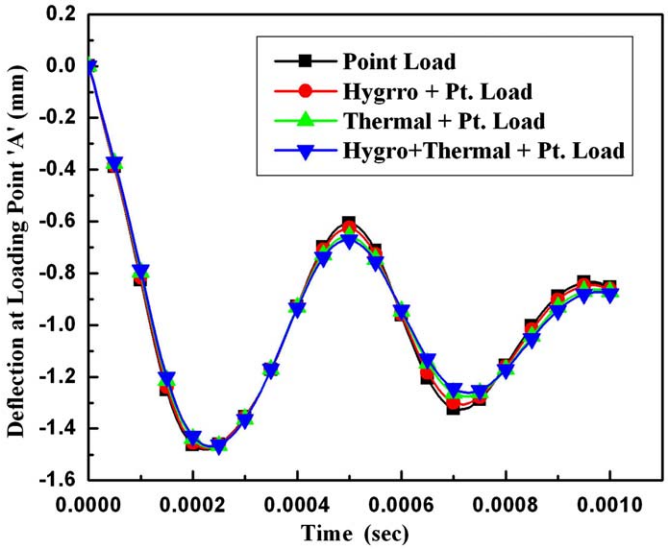


**Fig. 5.** Deflection at loading point 'A' of square panel of Fig. 2 for four situations (fiber angle is zero).

## 4. Results

Having substantiated COMDO8's reliability for such dynamic problems, attention now turns to optimizing the fiber direction locally to improve performance. Numerical optimizations, in conjunction with nonlinear dynamic FEA of the clamped square panel of Fig. 2 operating in a hygrothermal environment, are carried out using the previously applied 8-noded quadratic isoparametric shell element. Fiber angle within individual elements of the studied orthotropic panel are independently controlled with GA to enhance mechanical capabilities either by minimizing maximum deflection (Case I) or the fundamental frequency (Case II). To the author's knowledge, all of the published literatures on the composite optimization of dynamics problems are limited to changing ply angle (but plies remain rectilinearly orthotropic throughout the component), individual thickness, stacking lay-up or damping. The advanced approach utilized here optimizes locally the fiber angle of each 3D shell element within an orthotropic panel. Results of fiber orientations throughout the panel, minimized deflection and fundamental frequency of the optimized panels are presented in Tables 2 and 3 and Figs. 6–14.

Table 2 shows the minimized transverse deflection at point 'A' in Fig. 2 for each of the situations analyzed. These deflections are compared with that of the initial rectilinear orthotropic panel ($\theta$=0°). About 60% of the initial deflection is reduced by optimizing the local fiber direction. The influence of moisture and/or temperature on the deflection is small. While the moisture and/or temperature have little influence on the deflection at point 'A' (be the plate rectilinear throughout or fiber orientation locally optimized) the hygro-thermo-mechanical loading combination has the smallest deflection in both analyses.

Figs. 6–9 depict optimized fiber orientations throughout the square panel of Fig. 2 for the various situations analyzed and described in the previous section. A common tendency of the fiber arrangements in these four situations is that individual fibers of the 16 elements comprising plate incline toward the location of the applied 100 N load. However, the fiber direction in element number 4 of Fig. 2 is habitually inconsistent with those of surrounding elements. This is because the fiber angle of element 4 has very little influence on the object function of transverse deflection at point 'A'. Fiber orientation has relatively little effect on the deflection of point 'A' within a certain fiber angle range. This phenomenon occurs in the three situations of (i) point load ($F_Z = -100$ N at point 'A') only (Fig. 6), (ii) point load ($F_Z = -100$ N at point 'B')+moisture ($\Delta M =$ 0.25%) (Fig. 7) and (iii) point load ($F_Z = -100$ N at point 'A')+ temperature ($\Delta T = 125$ K) (Fig. 8). The optimized fiber angle of element 1 in situation (iv) of Table 2 and Fig. 9 is −43.72°. This deviates significantly from the fiber alignment trends of the surrounding elements. Several tests, each involving a different fiber angle of element 1, were performed by the author to assess the reliability and accuracy of the GA optimization. However these trials did not improved the solutions. Fig. 10 shows the dynamic responses at point 'A' of the square panel after locally optimizing the fiber angle with GA. The maximum deflection of the first oscillation of Fig. 10 is

**Table 2**
Effect of locally optimizing fiber orientation using GA on deflection at loading point 'A' of panel of Fig. 2.

| Situation | Loading conditions | Transverse deflection at point 'A' (mm) | |
|---|---|---|---|
| | | Initial rectilinear orthotropy ($\theta = 0°$) | Locally optimized fiber direction |
| (i) | Point load ($F_z = -100$ N) | −1.4797 | −0.6097 |
| (ii) | Hygro ($\Delta M = 0.25\%$)+Point load ($F_z = -100$ N) | −1.4762 | −0.6191 |
| (iii) | Thermal ($\Delta T = 125$ K)+Point load ($F_z = -100$ N) | −1.4726 | −0.6127 |
| (iv) | Hygro ($\Delta M = 0.25\%$)+Thermal ($\Delta T = 125$ K)+Point load ($F_z = -100$ N) | −1.4686 | −0.5996 |

**Table 3**
Effect of locally optimizing fiber orientation using GA on minimizing fundamental frequency ($f_1$) of panel of Fig. 2.

| Situation | Loading conditions | Fundamental frequency ($f_1$) | |
|---|---|---|---|
| | | Initial rectilinear orthotropy ($f_1$) (Hz) ($\theta = 0^\circ$) | Locally optimized fiber direction frequency ($f_1$) (Hz) |
| (i) | Free | 1.9339E+03 | 4.008E+02 |
| (ii) | Hygro ($\Delta M = 0.25\%$) | 1.9473E+03 | 5.145E+02 |
| (iii) | Thermal (425 K: $\Delta T = 125$ K) | 1.9309E+03 | 5.262E+02 |
| (iv) | Hygro ($\Delta M = 0.25\%$)+Thermal (425 K: $\Delta T = 125$ K) | 1.9443E+03 | 5.793E+02 |

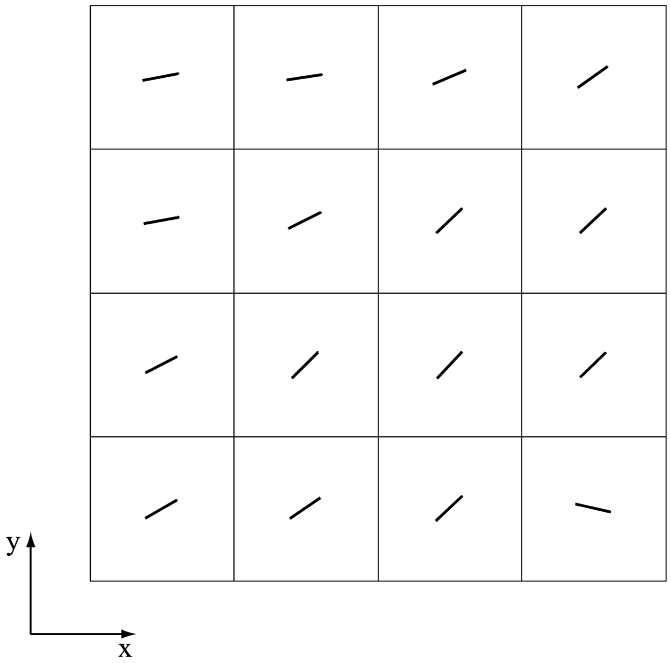


**Fig. 6.** Optimized local fiber angles to minimize transverse deflection at point 'A' (point load ($F_z = -100$ N) only).

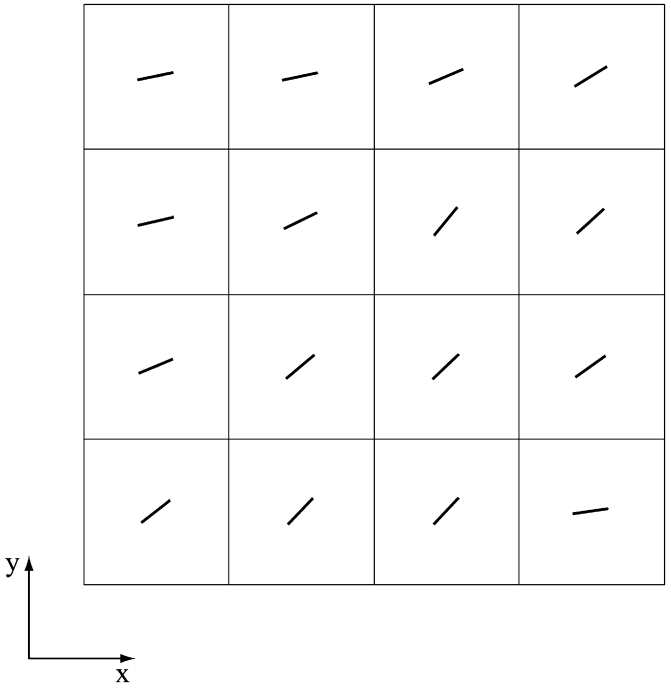


**Fig. 7.** Optimized local fiber angles to minimize transverse deflection at point 'A' (hygro ($\Delta M = 0.25\%$)+point load ($F_z = -100$ N)).

nearly the same for all the situations, but the differences (due to different environments) are greater in the second and third oscillation than that of the first.

The results of the second optimization case, i.e., minimizing the fundamental frequency ($f_1$) for the four situations analyzed: (i) free, (ii) moisture ($\Delta M = 0.25\%$), (iii) temperature ($\Delta T = 125$ K) and (iv) moisture ($\Delta M = 0.25\%$)+temperature ($\Delta T = 125$ K) are presented in Table 3 and Figs. 11–14. Determination of the fiber directions of each element here was handled in the same manner with the displacement optimization analysis. Table 3 contains comparative results of fundamental frequencies obtained by the subspace iteration method (Bathe, 1982) when all fiber angles are initially zero and fiber angles are optimized within individual elements by GA hybridizing FEA. The values of $f_1$ for optimized models are about one fourth those of the initial (rectilinear orthotropy throughout) panel. The optimized fiber arrangements are illustrated in Figs. 11–14. Fibers in all elements for the optimized free condition (i), Fig. 11, have approximately 90° fiber angle. On the other hand, for $\Delta M = 0.25\%$ situation (ii) of Table 3, fiber orientations of the eight elements adjacent to the clamped edge are essentially aligned with y-axis, and fibers of the other right-most eight elements remain at zero degree. Such a dramatic fiber-angle change within a certain uniform boundary also occurs in the thermal, situation (iii) (Fig. 13), and hygrothermal environment, situation (iv) (Fig. 14). For the thermal and hygrothermal situations, the fibers of elements 1, 5, 9, 13 of Fig. 2 and as shown in Fig. 13 and 14, become rearranged to about 90°.

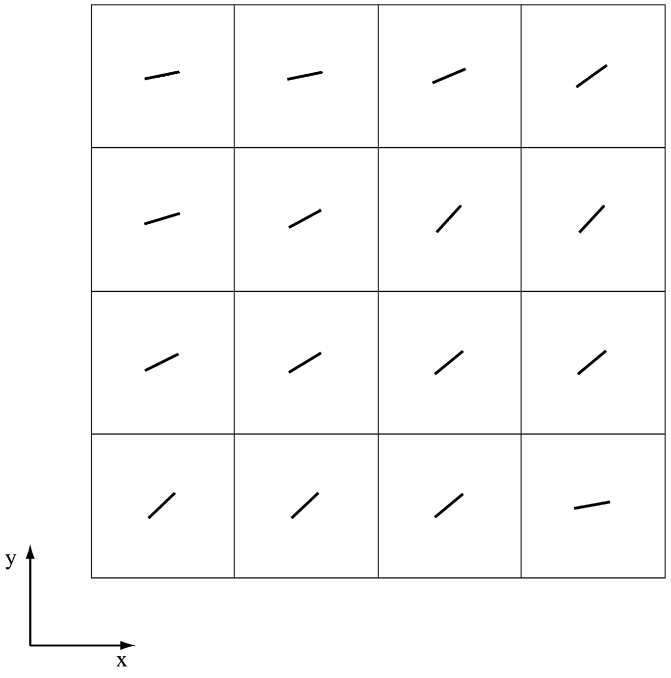


**Fig. 8.** Optimized local fiber angles to minimize transverse deflection at point 'A' (thermal ($\Delta T = 125$ K)+point load ($F_z = -100$ N)).

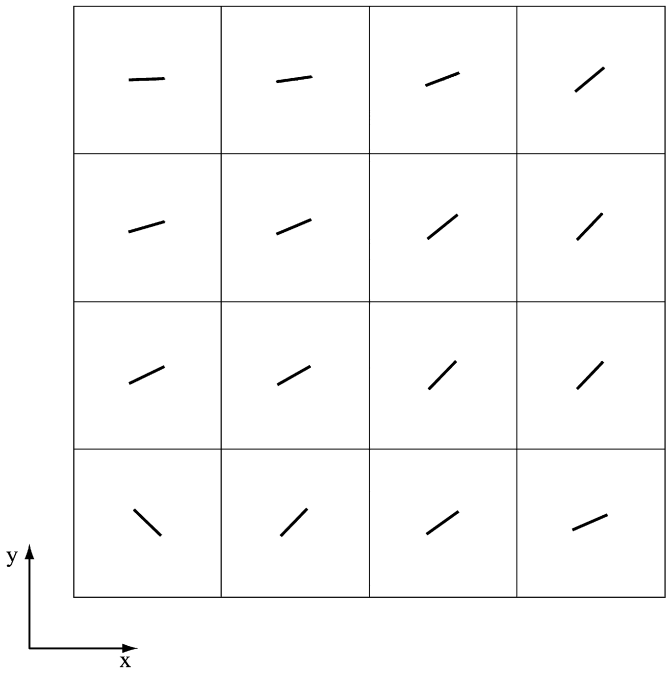


**Fig. 9.** Optimized local fiber angles to minimize transverse deflection at point 'A' (hygro ($\Delta M = 0.25\%$)+thermal ($\Delta T = 125\,\mathrm{K}$)+point load ($F_z = -100\,\mathrm{N}$)).

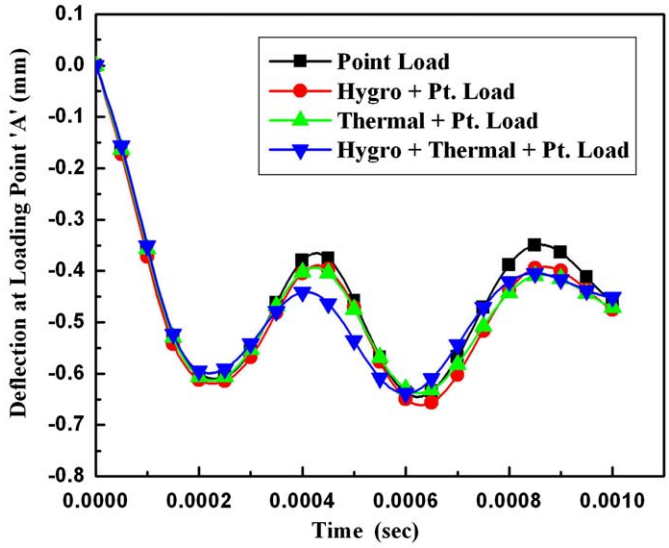


**Fig. 10.** Nonlinear dynamic responses of four situations analyzed with optimized local fiber directions to minimize transverse deflection at point 'A'.

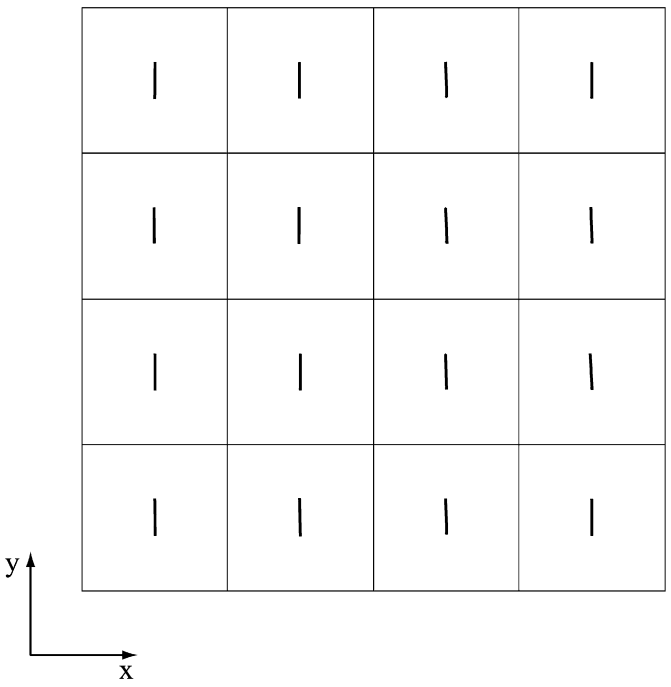


**Fig. 11.** Optimized local fiber angle distribution to minimize fundamental frequency ($f_1$) (free).

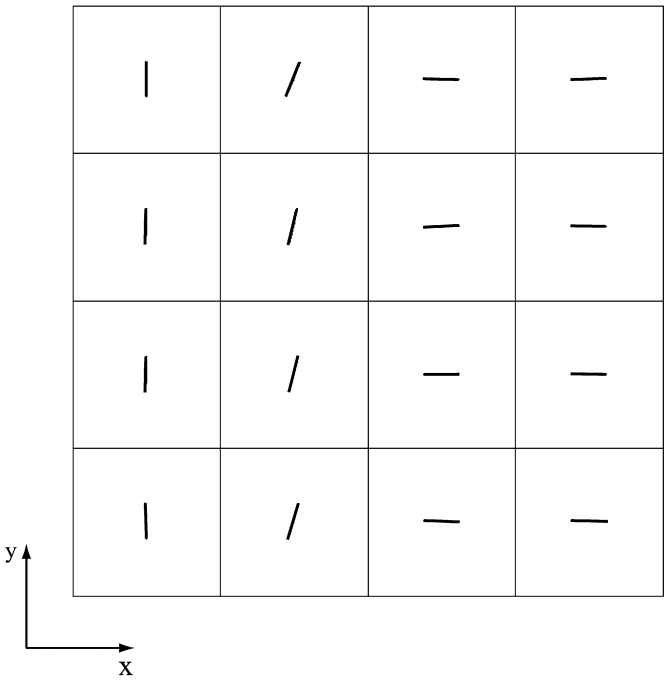


**Fig. 12.** Optimized local fiber angle distribution to minimize fundamental frequency ($f_1$) ($\Delta M = 0.25\%$).

As expected, the free-state panel has the lowest frequency (particularly when optimized), Table 3. Moisture and temperature increase the global stiffness. The thereby stiffer structure has higher first natural frequencies, (for the same material properties and boundary conditions). Fig. 15 demonstrates frequency variations according to the fiber angle change in which all of the elements have the same fiber angles.

## 5. Conclusion

The contribution of this paper is placed on the following three parts: (1) the development of transient nonlinear dynamic FEA equilibrium equation for 3D shell element that includes the hygrothermal behaviors together with mechanical load, (2) dynamic responses are optimized by controlling the fiber orientation locally within a ply of the individual elements. This technique has never been tried in other literatures, and (3) hygrothermally induced pre-stress is given as an initial condition for the calculation of the fundamental natural frequency and then the value was extremized by varying individual element's fiber direction. A FEA code coupled with GA enables one

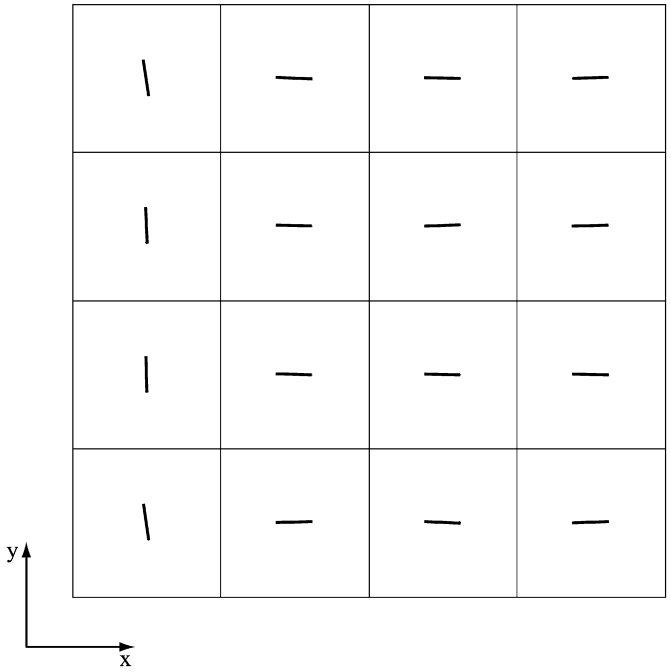


**Fig. 13.** Optimized local fiber angle distribution to minimize fundamental frequency ($f_1$) ($\Delta T = 125$ K).

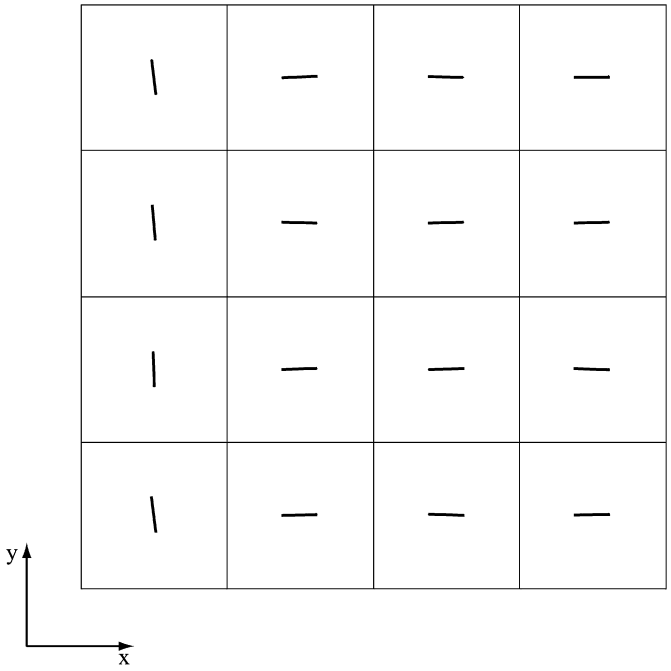


**Fig. 14.** Optimized local fiber angle distribution to minimize fundamental frequency ($f_1$) ($\Delta M = 0.25\%$+$\Delta T = 125$ K).

to extend the application to a highly numerical noised optimization problem as like the presented problem.

Most previous optimization dynamic studies of composite laminates are restricted to only mechanical loads, and dynamic analyses in hygrothermal environment are based on plate theory. The present extension to three-dimensional shell theory overcomes limitations of plate theory and hygrothermal constraints, thereby extending applicability. The implicit Newmark average acceleration method, in conjunction with the iterative incremental modified Newton–Raphson

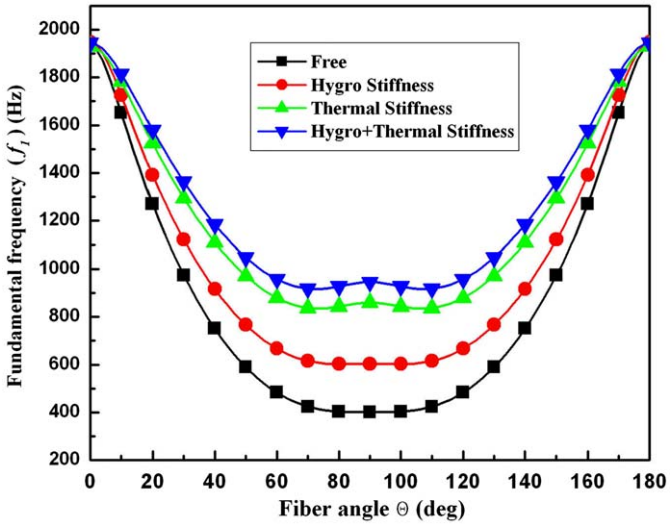


**Fig. 15.** Fundamental frequency ($f_1$) vs. common fiber angle $\theta_i$ throughout all elements of the plate of Fig. 2.

method, is successfully used with the present FEA for optimization. Dynamic component responses of displacement and fundamental frequency are minimized here by optimizing local fiber angles using GA. The GA optimization and FEM capabilities are combined into a software program called COMDO8. The present method can outperform earlier conventional design approaches. The latter typically omit moisture and/or temperature effects, and tend to be restricted to simple boundary conditions of flat, plate-like geometries. The current method can be extended to analyze arbitrarily shaped components subjected to complicated environmental conditions.

## Acknowledgment

The author wish to acknowledge the support of Satellite Technology Research Center of KAIST Project STSAT-3.

## Appendix.

Strain displacement transformation matrix

$$B_{L0} = \begin{bmatrix} N_{1,1} & 0 & N_{2,1} & 0 & \cdots & N_{N,1} & 0 \\ 0 & N_{1,2} & 0 & N_{2,2} & \cdots & 0 & N_{1,2} \\ N_{1,2} & N_{1,1} & N_{2,2} & N_{2,1} & \cdots & N_{N,2} & N_{N,1} \\ \dfrac{N_1}{\bar{x}_1} & 0 & \dfrac{N_2}{\bar{x}_1} & 0 & \cdots & \dfrac{N_N}{\bar{x}_1} & 0 \end{bmatrix}$$

$$\bar{x}_1 = \sum_{k=1}^{N} N_k x_1^k$$

$$B_{NL} = \begin{bmatrix} N_{1,1} & 0 & N_{2,1} & 0 & \cdots & N_{N,1} & 0 \\ N_{1,2} & 0 & N_{2,2} & 0 & \cdots & N_{N,2} & 0 \\ 0 & N_{1,1} & 0 & N_{2,1} & \cdots & & N_{N,1} \\ 0 & N_{1,2} & 0 & N_{2,2} & \cdots & & N_{N,2} \\ \dfrac{N_1}{\bar{x}_1} & 0 & \dfrac{N_2}{\bar{x}_1} & 0 & \cdots & \dfrac{N_N}{\bar{x}_1} & 0 \end{bmatrix}$$

## References

[1] N.V. Swamy Haidu, P.K. Sinha, Nonlinear transient analysis of laminated composite shells in hygrothermal environments, Compos. Struct. 72 (2006) 280–288.

[2] P.K. Parhi, S.K. Bhattacharyya, P.K. Sinha, Hygrothermal effects on the dynamic behavior of multiple delaminated composite plates and shells, J. Sound Vib. 248 (2001) 195–214.
[3] Y.S. Lee, Y.W. Lee, M.S. Na, Optimal design of hybrid laminated composite plates with dynamic and static constraints, Comput. Struct. 50 (1994) 797–803.
[4] M.E. Fares, Y.G. Youssif, A.E. Alamir, Minimization of the dynamic response of composite laminated doubly curved shells using design and control optimization, Compos. Struct. 59 (2003) 369–383.
[5] K.S. Sai Ram, P.K. Sinha, Hygrothermal effects on the free vibration of laminated composite plates, J. Sound Vib. 158 (1992) 133–148.
[6] S.A. Falco, S.M.B. Afonso, L.E. Vaz, Analysis and optimal design of plates and shells under dynamic loads—I: finite element and sensitivity analysis, J. Int. Soc. Struct. Multidiscipl. Optim. 27 (2004) 189–196.
[7] Y.M. Haddad, J. Feng, On the optimization of the mechanical behavior of a class of composite systems under both quasi-static and dynamic loading, J. Mater. Process. Tech. 119 (2001) 222–228.
[8] N. Alam, N.T. Asnsni, Vibration and damping analysis of fibre reinforced composite material plates, J. Compos. Mater. 20 (1986) 3–17.
[9] M.E. Fares, Y.G. Youssif, A.E. Alamir, Design and control optimization of composite laminated truncated conical shells for minimum dynamic response including transverse shear deformation, Compos. Struct. 64 (2004) 139–150.
[10] C.H. Shel, G.S. Springer, Moisture absorption and desorption of composite material, J. Compos. Mater. 10 (1976) 2–20.
[11] S.Y. Lee, W.J. Yen, Hygrothermal effects on the stability of a cylindrical composite shell panel, Comput. Struct. 33 (1989) 551–559.
[12] H.K. Cho, R.E. Rowlands, Maximizing buckling strength of perforated composite laminates by optimizing fiber orientation using genetic algorithm, in: ASME International Mechanical Engineering Congress and Exposition, Chicago, IL, 2006, pp. 5–10.
[13] H.K. Cho, R.E. Rowlands, Optimizing fiber direction in perforated orthotropic media to reduce stress concentration, J. Compos. Mater. 43 (2009) 1177–1198.
[14] M.K. Philippe Darnis, E. Ramahefarison, Optimization of laminated composites under static and dynamic constraints, Eng. Syst. Des. Anal. 8 (1994) 147–159.
[15] Z. Gürdal, R.T. Haftka, P. Hajela P., Design and Optimization of Laminated Composite Materials, Wiley, New York, 1971.
[16] G. Soremekun, Z. Gürdal, R.T. Haftka, L.T. Watson, Composite laminate design optimization by genetic algorithm with generalized elitist selection, Comput. Struct. 79 (2001) 131–143.
[17] J.H. Holland, Genetic algorithms and machine learning, Mach. Learn. 3 (1988) 95–99.
[18] D.E. Goldberg, Genetic Algorithms in Search Optimization and Machine Learning, Addison Wesley, New York, 1989.
[19] D.B. Adams, L.T. Watson, Z. Gürdal, C.M. Anderson-Cook, Genetic algorithm optimization and blending of composite laminates by locally reducing laminate thickness, Adv. Eng. Soft. 35 (2004) 35–43.
[20] H.K. Cho, R.E. Rowlands, Reducing tensile stress concentration in perforated hybrid laminate by genetic algorithm, Compos. Sci. Tech. 67 (2007) 1877–2883.
[21] K.J. Bathe, Finite Element Procedures in Engineering Analysis, Prentice-Hall, New York, 1982.
[22] G.H. Staab, Laminar Composites, Butterworth-Heinemann, Boston, 1999.
[23] R.D. Cook, D.S. Malkus, M.E. Plesha, R.J. Witt, Concepts and Applications of Finite Element Analysis, third ed., Wiley, New York, 2001.
[24] J.N. Reddy, Mechanics of Laminated Composite Plates: Theory and Analysis, CRC, New York, 1997.
[25] O.C. Zienkiewicz, R.L. Taylor, The Finite Element Method, fourth ed., McGraw-Hill, New York, 1991.
[26] T.Y. Chang, K. Sawamiphakdi, Large deformation analysis of laminated shells by finite element method, Comput. Struct. 13 (1981) 331–340.